

# Transverse Faraday-Rotation Gradients Across the Jets of 15 Active Galactic Nuclei

D. C. Gabuzda, S. Knuettel & B. Reardon

*Physics Department, University College Cork, Cork, Ireland*

## ABSTRACT

The presence of a helical magnetic field threading the jet of an Active Galactic Nucleus (AGN) should give rise to a gradient in the observed Faraday rotation measure (RM) across the jet, due to the associated systematic change in the line-of-sight magnetic field. Reports of observations of transverse RM gradients across AGN jets have appeared in the literature starting from 2002, but concerns were raised about the resolution required for these gradients to be reliable, and there was a lack of a full understanding of the best approach to accurate estimation of the uncertainties of local RM values. These questions have now been resolved by recent Monte Carlo simulations carried out by various groups, enabling both a verification of previously published results and reliable analyses of new data. We consider here RM gradients across the jet structures of 15 AGN, some previously published in the refereed literature but without a correct and complete error analysis, and some published for the first time here, all of which have monotonic transverse RM gradients with significances of at least  $3\sigma$ .

**Key words:**

## 1 INTRODUCTION

The radio emission associated with Active Galactic Nuclei (AGNs) is synchrotron emission, which can be linearly polarized up to about 75% in optically thin regions, where the polarization angle  $\chi$  is orthogonal to the projection of the magnetic field  $\mathbf{B}$  onto the plane of the sky, and up to 10–15% in optically thick regions, where  $\chi$  is parallel to the projected  $\mathbf{B}$  (Pacholczyk 1970). Linear polarization measurements thus provide direct information about both the degree of order and the direction of the  $\mathbf{B}$  field giving rise to the observed synchrotron radiation.

Multi-frequency Very Long Baseline Interferometry (VLBI) polarization observations also provide information about the parsec-scale distribution of the spectral index (optical depth) of the emitting regions, as well as Faraday rotation occurring between the source and observer. Faraday rotation of the plane of linear polarization occurs during the passage of the associated electromagnetic wave through a region with free electrons and a  $\mathbf{B}$  field with a non-zero component along the line of sight. When the Faraday rotation occurs outside the emitting region in regions of non-relativistic (“thermal”) plasma, the amount of rotation is given by

$$\chi_{obs} - \chi_o = \frac{e^3 \lambda^2}{8\pi^2 \epsilon_o m^2 c^3} \int n_e \mathbf{B} \cdot d\mathbf{l} \equiv \text{RM} \lambda^2 \quad (1)$$

where  $\chi_{obs}$  and  $\chi_o$  are the observed and intrinsic polarization angles, respectively,  $-e$  and  $m$  are the charge and mass

of the particles giving rise to the Faraday rotation, usually taken to be electrons,  $c$  is the speed of light,  $n_e$  is the density of the Faraday-rotating electrons,  $\mathbf{B}$  is the magnetic field,  $d\mathbf{l}$  is an element along the line of sight,  $\lambda$  is the observing wavelength, and RM (the coefficient of  $\lambda^2$ ) is the Rotation Measure (e.g., Burn 1966). Simultaneous multifrequency observations thus allow the determination of both the RM, which carries information about the electron density and the line-of-sight  $\mathbf{B}$  field in the region of Faraday rotation, and  $\chi_o$ , which carries information about the intrinsic  $\mathbf{B}$ -field geometry associated with the source projected onto the plane of the sky.

As was pointed out by Blandford (1993), the presence of a helical  $\mathbf{B}$  field threading the jet of an AGN should give rise to a gradient in the observed RM across the jet, due to the associated systematic change in the line-of-sight  $\mathbf{B}$  field. Further, such fields would come about in a natural way as a result of the “winding up” of an initial “seed” field by the rotation of the central accreting objects (e.g. Nakamura et al. 2001; Lovelace et al. 2002).

The first report of an actual detection of such a transverse RM gradient was made by Asada et al. (2002), for the VLBI jet of 3C273; this result was later confirmed by Zavala & Taylor (2005) and Hovatta et al. (2012). Transverse RM gradients were subsequently reported across the parsec-scale jets of a number of other AGN (e.g., Gabuzda et al. 2004, 2008; Asada et al. 2008, 2010; Kharb et al. 2009; Mahmud et al. 2009; Croke et al. 2010), and interpreted as reflecting

the systematic change in the line-of-sight component of a toroidal or helical jet  $\mathbf{B}$  field across the jets.

However, there were three main difficulties with these measurements, which led to skepticism about these results among some researchers. One was that it seemed non-intuitive that it could be possible to detect these RM gradients when the intrinsic widths of the jets were sometimes appreciably smaller than the widths of the beams with which they were observed; this was expressed by Taylor & Zavala (2010) through their proposed criterion that an observed transverse RM gradient must have a width of at least three “resolution elements” (usually taken to mean three beamwidths) in order to be considered reliable. This criterion was presented without justification, but if it was correct, it would invalidate nearly all the previously published reports of transverse RM gradients, as well as make it very difficult to identify new cases.

The second difficulty was that determining the significance of observed gradients required reasonably accurate estimation of the uncertainties in the RM value being compared. The standard practice at the time was to assign an uncertainty to the Stokes  $Q$  and  $U$  values in individual pixels equal to the off-source rms in the corresponding  $Q$  and  $U$  images,  $\sigma_{Q,rms}$  and  $\sigma_{U,rms}$ , then propagate these uncertainties to determine the corresponding uncertainties in the polarization angles  $\chi = 0.5 \arctan U/Q$ ; however, this approach had never been tested. In addition, attempts were made to assign uncertainties to RM values averaged over several pixels based on the standard deviation of the values being averaged, but this ignored the presence of correlations in the values measured in nearby pixels due to convolution with the CLEAN beam used. Further, residual instrumental polarizations remaining in the polarization data after calibration could potentially add additional uncertainty to the measured polarization angles, and this had not been taken into account.

A third difficulty was that there can, in some cases, be small but significant relative shifts between the polarization angle images obtained at different frequencies, due to the frequency dependence of the position of the VLBI core (Blandford & Königl 1979). This led to concerns about whether apparent Faraday rotation gradients could arise due to incorrect relative alignment of the polarization images. The necessary shifts can be determined and corrected for, but this had not been done in a number of studies.

Thus, there was a need to clarify whether there was a minimum resolution required to reliably detect Faraday-rotation structure, to identify a suitable approach for accurately estimating uncertainties in quantities at individual locations in VLBI images and to ensure that any small relative shifts between the polarization angle images used to construct the RM maps were correctly taken into account (or that they were small enough for their effect on the RM images to be negligible).

A first important step was taken by Hovatta et al. (2012), who carried out Monte Carlo simulations based on realistic “snapshot” baseline coverage for VLBA observations at 7.9, 8.4, 12.9 and 15.4 GHz, aimed at investigating

the statistical occurrence of spurious RM gradients across jets with intrinsically constant polarization profiles. Inspection of the right-hand panel of Fig. 30 of Hovatta et al. (2012) shows that the fraction of spurious  $3\sigma$  gradients was no more than about 1%, even for the smallest observed RM-gradient widths they considered, about 1.4 beamwidths. Relatively few  $2\sigma$  gradients were also found, although this number reached about 7% for observed jet widths of about 1.5 beamwidths; nevertheless, Hovatta et al. (2012) point out that  $2\sigma$  gradients are potentially also of interest if confirmed over two or more epochs.

The results of Hovatta et al. (2012) have also now been confirmed by similar Monte Carlo simulations carried out by Algaba (2013) for simulated data at 12, 15 and 22 GHz and by Murphy & Gabuzda (2013) for simulated data at 1.38, 1.43, 1.49 and 1.67 GHz and at the same frequencies as those considered by Hovatta et al. (2012). The 1.38-1.67 GHz frequency range considered by Murphy & Gabuzda (2013) yielded a negligible number of spurious  $3\sigma$  gradients (and fewer than 1% spurious  $2\sigma$  gradients), even for observed jet widths of only 1 beamwidth (i.e., for poorly resolved jets).

Two more sets of Monte Carlo simulations based on realistic snapshot VLBA baseline coverage adopted a complementary approach: instead of considering the occurrence of spurious RM gradients across jets with constant polarization, they considered simulated jets with various widths and with transverse RM gradients of various strengths, convolved with various size beams. Mahmud et al. (2013) carried out such simulations for 4.6, 5.0, 7.9, 8.4, 12.9 and 15.4 GHz VLBA data, and Murphy & Gabuzda (2013) for 1.38, 1.43, 1.49 and 1.67 GHz VLBA data. These simulations clearly showed that, with realistic noise and baseline coverage, the simulated RM gradients could remain clearly visible, even when the jet width was as small as  $1/20$  of a beam width.

All these simulations clearly demonstrate that the width spanned by an RM gradient is not a crucial criterion for its reliability, at least down to  $1/20$  of a beam width. This counterintuitive result essentially comes about because polarization is a vector quantity, while the intensity is a scalar. A difference in the polarization angles across the jet can be detected in situations where intensity structure could not be. Alternatively, thinking of the polarization as being composed of Stokes  $Q$  and  $U$ , this enhanced sensitivity to closely spaced structures comes about because both  $Q$  and  $U$  can be positive or negative. It is important to bear in mind that we are not speaking here of being able to accurately deconvolve the observed RM profiles to determine the intrinsic transverse RM structure — only of the ability to detect the presence of a systematic transverse RM gradient.

Another key outcome of the Monte Carlo simulations of Hovatta et al. (2012) is an empirical formula that can be used to estimate the uncertainties in intensity (Stokes  $I$ ,  $Q$  or  $U$ ) images, including the uncertainty due to residual instrumental polarization (“D-terms”) that has been incompletely removed from the visibility data. In regions of source emission where the contribution of the residual instrumental polarization is negligible, the typical uncertainties in individual pixels are approximately 1.8 times the rms deviations of the flux about its mean value far from regions of source emission,  $\sigma_{rms}$ . This is roughly a factor of two greater than the uncertainties that have been assigned to

Table 1: Source properties							
Source	Redshift	Optical ID	pc/mas	Ref	Integrated RM (rad/m <sup>2</sup> )	Ref	Original RM Map Ref
0256+075	0.89	BL	7.78	S89, KS90	-13	P	*
0355+508	1.52	Q	8.54	M	-17	R	ZT
0735+178	0.45	BL	5.73	M	+9	R	G2
0745+241	0.41	HPQ	5.42	M	+21	P	G1
0748+126	0.89	Q	7.78	M	+14	T	ZT
0820+225	0.95	BL	7.93	S93, KS90	+81	P	G1
0823+033	0.50	BL	6.12	M	+1	P	*
1156+295	0.72	HPQ	7.25	M	-32	T	G2
1219+285	0.10	BL	1.87	M	-1	R	*
1334-127	0.54	HPQ	6.33	M	-23	P	*
1652+398	0.034	BL	0.66	M	+42	R	G1
1749+096	0.32	BL	4.64	M	+94	P	G2
1807+698	0.051	BL	0.98	M	+11	T	G1
2007+777	0.34	BL	4.83	M	-20	R	*
2155-152	0.67	HPQ	7.02	M	+19	P	*

BL = BL Lac object; Q = Quasar with no optical polarization data; HPQ = Quasar with fractional linear polarization in the optical above 3% on at least one occasion; M = MOJAVE website; S89 = Stickel et al. 1989; S93 = Stickel et al. 1993; KS90 = Kühr & Schmidt 1990; R = Rusk 1988; P = Pushkarev 2001; T = Taylor et al. 2009; ZT = Zavala & Taylor (2004); G1 = Gabuzda et al. (2004); G2 = Gabuzda et al. (2008); \* = Not previously published in the refereed literature

Table 2: Map properties							
Source	Figure	Freq (GHz)	Peak (Jy)	Lowest contour (%)	BMaj (mas)	BMin (mas)	BPA (deg)
0256+075	1a	4.6	0.38	0.25	3.35	1.69	-3.2
0355+508	3a	8.1	4.42	0.50	1.98	0.94	21.7
0748+126	3b	8.1	0.90	0.25	2.25	0.86	-7.7
0823+033	1b	5.0	1.16	0.25	3.67	1.64	-0.1
1219+285	1c	5.0	0.28	0.50	3.68	2.58	-13
1334-127	2a	4.6	3.30	0.25	3.76	1.49	-0.9
1334-127	2d	4.6	3.27	0.25	2.00	2.00	0
2007+777	1d	5.0	0.95	0.25	1.82	1.66	-20.4
2155-152	2b,c	4.6	1.02	0.25	4.24	1.68	-1.7
2155-152	2e	4.6	1.01	0.50	2.66	2.66	0

intensities measured in individual pixels as standard practice in past studies, indicating that the past uncertainties have been somewhat underestimated. These results have recently been confirmed by the Monte Carlo simulations of Coughlan (2014), which likewise indicate that the typical intensity uncertainties in individual pixels are of order twice the off-source rms, with significant pixel-to-pixel variations in the uncertainties appearing in the case of well resolved sources.

New Faraday-rotation analyses based on the error formulation of Hovatta et al. (2012), focusing on monotonicity and a significance of at least  $3\sigma$  as the key criteria for reliability of observed transverse RM gradients, and ensuring that the RM images analyzed are not significantly affected by relative shifts between the polarization-angle images at different frequencies have begun to appear (Mahmud et al. 2013, Gabuzda et al. 2014a, 2014b).

There is also a need to verify the reliability of previously published results. In the current paper, we present the results of new analyses of the 7 RM maps previously published by Gabuzda et al. (2004, 2008), and confirm that the previously reported RM gradients are significant. We also report

8 new cases of monotonic, statistically significant transverse RM gradients across AGN jets, based on both published maps and maps not previously published in the refereed literature, constructed using a variety of datasets with three to seven frequencies.

## 2 OBSERVATIONS

We consider here both new analyses of previously published Faraday RM maps and RM images published here for the first time. In all cases, the observations were obtained on the NRAO Very Long Baseline Array. We have applied the error estimation formula of Hovatta et al. (2012) to determine the uncertainties in the polarization angles in individual pixels.

The observed Faraday rotation occurs predominantly in two locations: in the immediate vicinity of the AGN and in our Galaxy. The latter contribution must be estimated and removed if we wish to isolate Faraday rotation occurring in the vicinity of the AGN itself. The effect of the integrated (Galactic) RM is usually small, but can be substantial for some sources, e.g. those lying near the plane of the Galaxy.

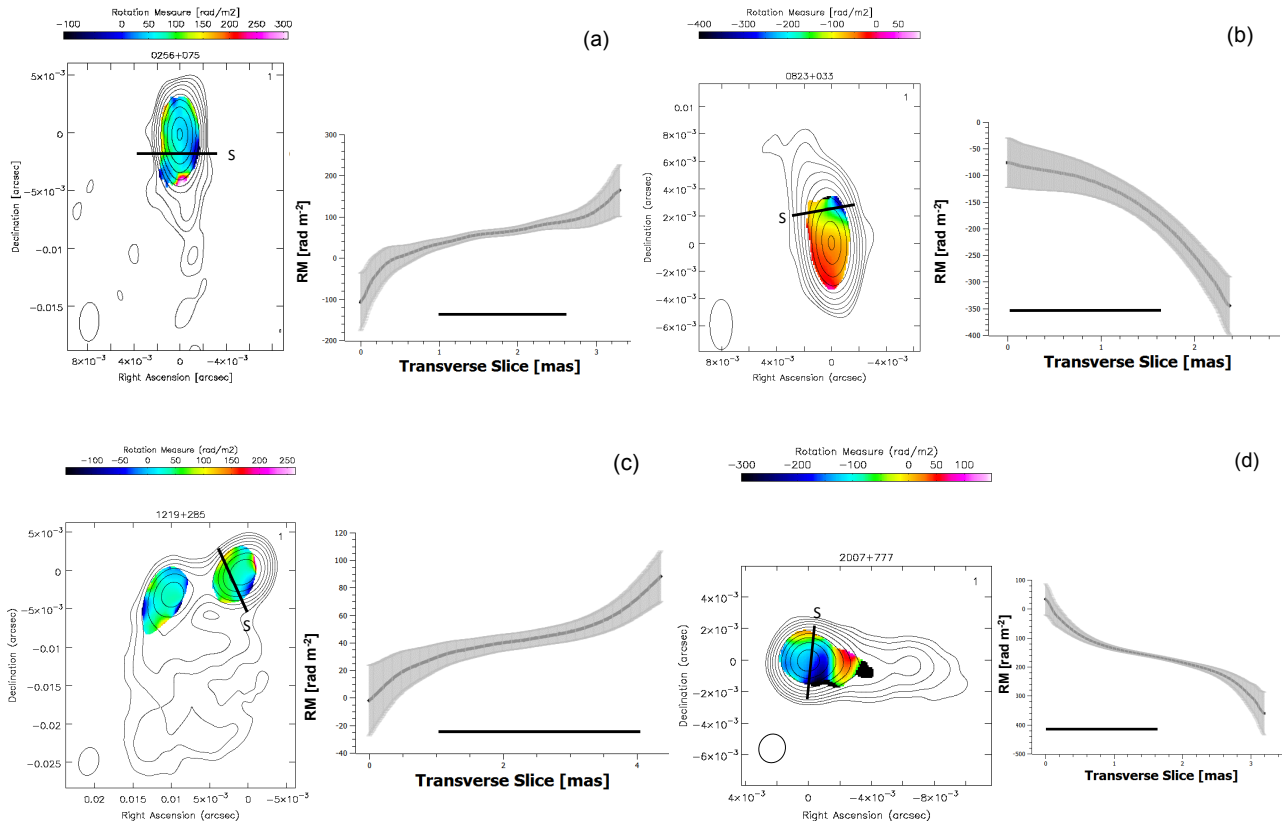


**Figure 1.** (a) 4.6-GHz intensity map of 0256+075 and 5.0-GHz intensity maps of (b) 0823+033, (c) 1219+285, and (d) 2007+777 with the corresponding RM distributions superposed (left panels). The lines drawn across the RM distributions show the locations of the RM slices shown in the corresponding right-hand panels; the letter “S” at one end of these lines marks the side corresponding to the starting point for the slice. The bold horizontal bars shown with the slice profiles indicate the beam full widths at half maximum in the direction of the slices, which are (a) 1.7 mas, (b) 1.65 mas, (c) 2.7 mas and (d) 1.7 mas.

We used various integrated RM measurements obtained using the Very Large Array, indicated in Table 1, to remove the effect of the Galactic RM from the observed polarization angles, when significant, before making our RM maps.

When required, we corrected for any significant relative shifts between the polarization angle images used to make the RM maps. We determined these relative shifts using the cross-correlation approach of Croke & Gabuzda (2008); the shifts were tested by making spectral-index maps taking into account the relative shifts, to ensure that they did not show any spurious features due to residual misalignment between the maps.

The maps were made with natural weighting. In a number of cases when the beams obtained were fairly elongated, we also made versions of the RM maps using circular beams with areas (roughly) equal to those of the intrinsic elliptical beams, to test the robustness of gradients detected in the original images.

### 2.1 5–15 GHz, February 1997

We consider the RM maps published by Gabuzda et al. (2004), as well as several RM maps for other objects for which data were taken in the same set of observations. These observations focused on objects in the sample of 34 BL Lac objects defined by Kühr & Schmidt (1990). The observa-

tions were carried out on 9th February 1997 at 5, 8.4 and 15 GHz. The procedures used to calibrate the data and construct the published RM maps are described by Gabuzda et al. (2004). When the original RM maps were published, no attempt to check the alignment of the polarization angle images at the three frequencies was made, and we correct this here. Gabuzda et al. (2004) removed the Galactic RM values from their RM maps; we have done this for the new RM maps analyzed here as well.

### 2.2 5–15 GHz, April 1997

Six compact BL Lac objects were observed with the VLBA on 6th April 1997, simultaneously at 22.2, 15.3, 8.4 and 5.0 GHz; we consider here only the lower three frequencies, since the difference in resolution between the 22-GHz and 5-GHz data is quite large. The procedures used to calibrate the data are described by Reynolds et al. (2001) and Gabuzda & Chernetskii (2003). The procedures used to construct the RM map for 1219+285 considered here were the same as those used by Gabuzda et al. (2004). We have taken into account the correct alignment between the polarization angle images at the different frequencies in the RM map presented here. We have not attempted to correct for the effect of Galactic Faraday rotation, as the integrated RM is negligible in this case ( $-1 \pm 3$  rad/m<sup>2</sup>; Rusk 1988).

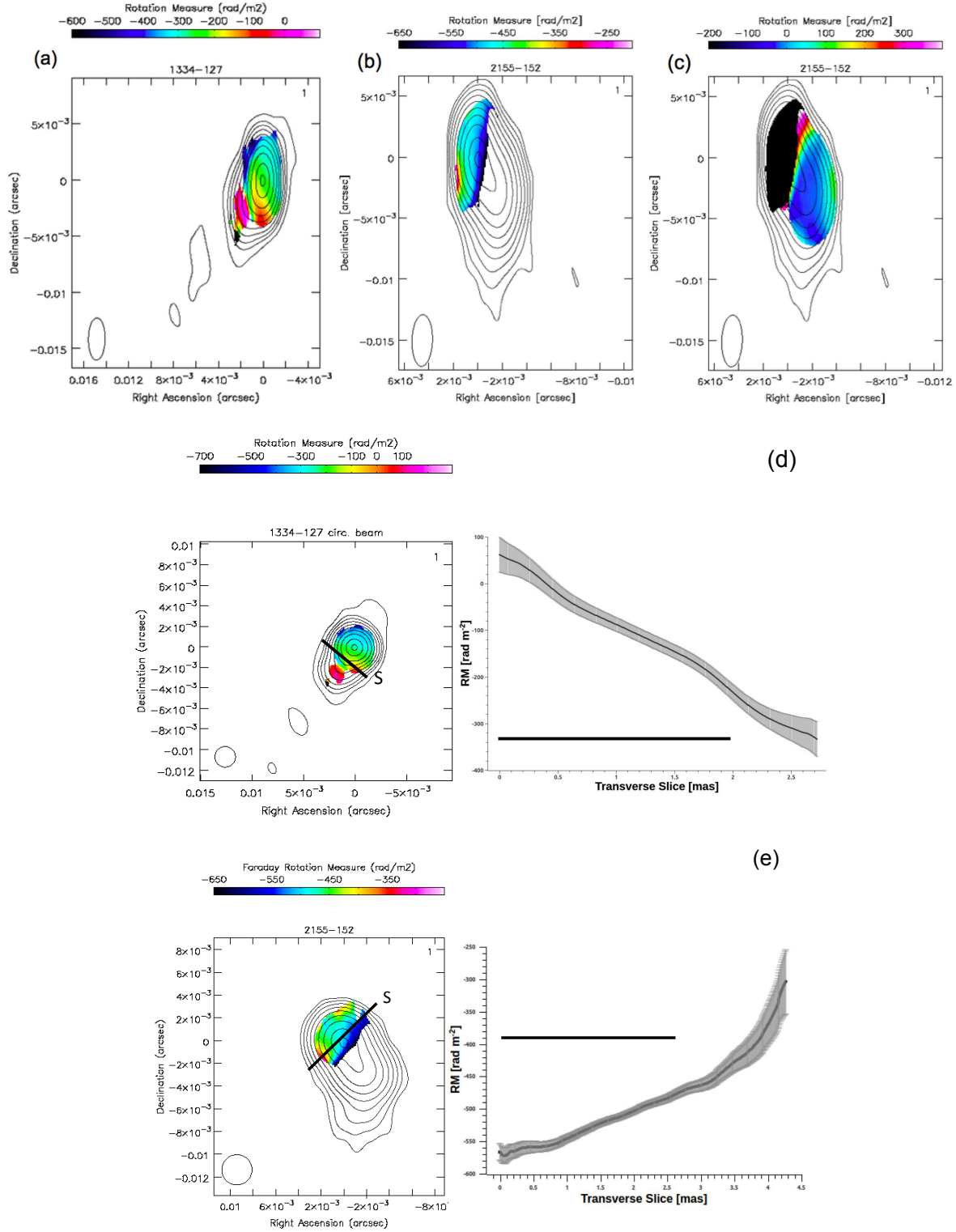


**Figure 2.** 4.6-GHz intensity maps of (a) 1334–127 (intrinsic beam), (b) 2155–152 core region (intrinsic beam), (c) 2155–152 jet (intrinsic beam), (d) 1334–127 (circular beam) (e) 2155–152 core region (circular beam). The lines drawn across the superposed RM distributions in panels (d) and (e) show the locations of the RM slices shown in the corresponding right-hand panels; the letter “S” at one end of these lines marks the side corresponding to the starting point for the slice. The bold horizontal bars shown with the slice profiles indicate the beam full widths at half maximum in the direction of the slices, which are (d) 2.0 mas and (e) 2.7 mas.

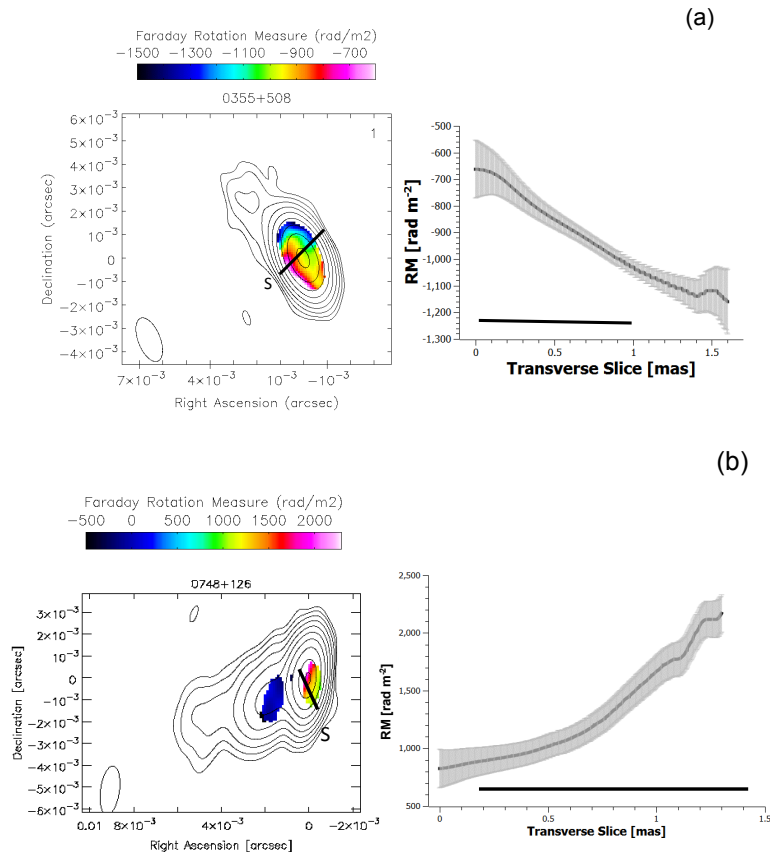


**Figure 3.** 8.1-GHz intensity maps of (a) 0355+508 and (b) 0748+126 with the corresponding RM distributions superposed (left panels). The lines drawn across the RM distributions show the locations of the RM slices shown in the corresponding right-hand panels; the letter “S” at one end of these lines marks the side corresponding to the starting point for the slice. The bold horizontal bars shown with the slice profiles indicate the beam full widths at half maximum in the direction of the slices, which are (a) 1.0 mas and (b) 1.3 mas.

### 2.3 8.1–15.2 GHz, June 2001

Zavala & Taylor (2004) present 15.2-GHz total intensity maps with superposed polarization sticks and Faraday RM maps based on 7 well-spaced frequencies between 8.1 and 15.2 GHz for 17 AGN. These observations were carried out on 20th June 2001 at 8.1, 8.2, 8.4, 8.6, 12.1, 12.6 and 15.2 GHz. The procedures used to calibrate the data and construct the published RM maps are described by Zavala & Taylor (2004). The final fully calibrated and self-calibrated visibility data were kindly provided by R. Zavala, and it is these data that we used to make the RM images analyzed here.

A visual inspection of the published RM images indicated the possible presence of transverse RM gradients across the jets of 0355+508 and 0748+126, as well as 1749+096, whose transverse RM gradient was previously reported by Gabuzda et al. (2008). We made Stokes  $Q$  and  $U$  maps in AIPS for each of these two sources at each of the frequencies, ensuring that the image parameters (cell size, image size, beam parameters) were the same for all 7 frequencies, and taking the errors to be given by the approach of Hovatta et al. (2012). We then used these to obtain matched-resolution polarization-angle (“PANG”) and polarization-angle noise (“PANGN”) images, which were used to construct RM maps after removing the effect of inte-

grated (Galactic) Faraday rotation when significant. These essentially reproduced the RM maps published by Zavala & Taylor (2004), but with the more conservative errors of Hovatta et al. (2012) and with the Galactic RM values removed.

Note that the procedure described above for matching the resolutions of the images at the different frequencies was different from the approach adopted by Zavala & Taylor (2004), who applied tapers to the 12 and 15 GHz data used to produce the polarization-angle maps so as to approximate the 8-GHz resolution, and then used a restoring beam matched to the 8-GHz beam. Although the procedure used by Zavala & Taylor (2004) is formally more correct, we did not find any significant differences between our RM maps and those of Zavala & Taylor (2004); it is likely that any differences in the polarization maps due to the application of these different approaches appear at lower flux and polarization levels than those contributing to the RM images.

No mention of image alignment is made in the original publication, and the published spectral-index maps suggest that no image alignment was done (they often show a band of seemingly optically thin emission on the side of the core opposite the jet); we have ensured correct alignment of the polarization-angle images in our analysis.

#### 2.4 4.6–15.1 GHz, August 2003, March 2004 and September 2004

We consider here the published RM maps of Gabuzda et al. (2008), as well as RM maps for several other objects for which data were taken in the same sets of observations. The observations were carried out at 4.6, 5.1, 7.9, 8.9, 12.9 and 15.4 GHz on 22nd August 2003, 22nd March 2004 and 10th September 2004. The procedures used to calibrate the data and construct the published RM maps are described by Gabuzda et al. (2008). When the original RM maps were published, no attempt to check the alignment of the polarization angle images at the three frequencies was made, and we address this here. Gabuzda et al. (2008) removed the Galactic RM values from their RM maps; we have done this for the new RM maps analyzed here as well.

### 3 RESULTS

The source names, redshifts, optical identifications, pc/mas values and integrated rotation measures are summarized in Table 1. The pc/mas were determined assuming a cosmology with  $H_o = 71 \text{ km s}^{-1} \text{ Mpc}^{-1}$ ,  $\Omega_\Lambda = 0.73$  and  $\Omega_m = 0.27$ ; the redshifts and pc/mas values were taken from the MOJAVE project website when available (<http://www.physics.purdue.edu/MOJAVE/>).

RM maps together with slices in regions of detected transverse RM gradients are shown in Figs. 1–3. The frequencies, peaks and bottom contours of the intensity maps shown in these figures are given in Table 2; in all cases, the contour levels increase in steps of a factor of two. The ranges of the RM maps are indicated by the colour wedges shown with the maps. For consistency, in each case, the RM slices were taken in the clockwise direction relative to the base of the jet (located upstream from the observed core). The lines drawn across the RM distributions show the locations of the slices; the letter “S” at one end of these lines marks the side corresponding to the starting point for the slice (a slice distance of 0). The slices were taken in regions where the significance of the RM gradients was highest. The full width at half maximum of the beam in the direction of the slice is shown together with the slices by a bold bar.

The statistical significance of transverse gradients detected in our RM maps are summarized in Table 3. When plotting the slices in Figs. 1–3 and finding the difference between the RM values at two ends of a gradient,  $\Delta\text{RM}$ , we did not include uncertainty in the polarization angles due to EVPA calibration uncertainty; this is appropriate, since EVPA calibration uncertainty affects all polarization angles for the frequency in question equally, and so cannot introduce spurious RM gradients, as is discussed by Mahmud et al. (2009) and Hovatta et al. (2012). The contribution of uncertainty in the polarization angles due to residual D-terms described by Hovatta et al. (2012) has been included. Hovatta et al. (2012) defined the uncertainty in  $\Delta\text{RM}$  to be the largest RM uncertainty at the edge of the jet; instead, we have taken the uncertainty  $\Delta\text{RM}$  to be the sum of the two RM uncertainties added in quadrature. While not strictly correct mathematically due to the effects of convolution, this at least takes into account the uncertainties at both ends of the slice, and is more conservative than the approach of Hovatta et al. (2012). In most cases, the RM values

used to calculate  $\Delta\text{RM}$  are located at or near the ends of the slices shown; in some cases, we used values somewhat farther from the ends of the slices because the increase in the uncertainties at the slice ends appreciably reduced the statistical significance of the RM difference. In all cases, the RM slices showed monotonic changes in the RM across the slices right to the slice ends.

Note that we do not reproduce the RM maps previously published by Gabuzda et al. (2004, 2008) here, as an initial analysis of the transverse RM structure was already carried out in those papers; however, our results for those sources are included in Table 3.

Results for each of the AGN considered here are summarized briefly below. We took a transverse RM gradient to be across the core if it was located within the 50% intensity contour; otherwise, we took the gradient to be across the jet.

#### 3.1 5–15 GHz, February 1997

These RM maps are based on simultaneous VLBA observations at 15, 8 and 5 GHz.

**0745+241.** This RM map was originally published by Gabuzda et al. (2004). Our results confirm that the previously reported RM gradient is monotonic; the significance of this transverse gradient is about  $4\sigma$ .

**0820+225.** This RM map was originally published by Gabuzda et al. (2004). Our results confirm that the previously reported RM gradient is monotonic; the significance of this transverse gradient is  $3.4\sigma$ .

**0823+033.** This RM map, shown in Fig. 1b, has not been published previously. It shows a monotonic transverse RM gradient with a significance of about  $4\sigma$ .

**1652+398.** This RM map was originally published by Gabuzda et al. (2004). Our results confirm that the previously reported RM gradient is monotonic; the significance of the transverse gradient is  $4.8\sigma$ . Note that a transverse RM gradient with the same direction on somewhat larger scales has been reported by Croke et al. (2010).

**1807+698.** This RM map was originally published by Gabuzda et al. (2004). Our results confirm that the previously reported RM gradient is monotonic; the significance of the transverse gradient is  $3.5\sigma$ .

**2007+777.** This RM map, shown in Fig. 1d, has not been published previously. It shows a monotonic transverse RM gradient with a significance of  $5.5\sigma$ .

#### 3.2 5–15 GHz, April 1997

**1219+285.** This RM map, shown in Fig. 1c, has not been published previously. It shows a monotonic transverse RM gradient with a significance of about  $3\sigma$ .

#### 3.3 8.1–15.2 GHz, June 2001

RM maps of these sources based on the same visibility data but with somewhat different weighting were originally published by Zavala & Taylor (2004). They were chosen for our

analysis because possible RM gradients across the jet structure are visible by eye in the RM maps of Zavala & Taylor (2004).

**0355+508.** Our map in Fig. 3a shows a monotonic transverse RM gradient across the core region, with a significance of  $4.2\sigma$ . The orientation of the beam in our image is roughly along the jet, making it possible that the significance of the gradient has been artificially increased by this effective averaging along the jet. The RM gradient remains visible when the RM map is made using a circular beam, with a significance of about  $3\sigma$ .

**0748+126.** Our map in Fig. 3b shows a transverse RM gradient across the core region, with a significance of nearly  $6\sigma$ .

### 3.4 4.6–15.1 GHz, August 2003, March 2004 and September 2004

**0256+075.** An RM map made from the same visibility data was published by Mahmud & Gabuzda (2008), but without any error analysis. Our map in Fig. 1a shows a monotonic transverse RM gradient across the inner jet, whose significance is  $2.9\sigma$ . We also made this RM map using a circular beam; the RM gradient remains visible, and its significance increases to  $3.2\sigma$ .

**0735+178.** An RM map made from the same visibility data was published by Gabuzda et al. (2008). Our analysis shows that the previously reported monotonic, transverse RM gradient across the jet has a significance of  $5.5\sigma$ .

**1156+295.** An RM map made from the same visibility data was published by Gabuzda et al. (2008). Our analysis shows that the previously reported monotonic, transverse RM gradient across the core region has a significance of  $5.8\sigma$ .

**1334–127.** Our map in Fig. 2 is the first RM map published for this source in this frequency range. It shows a nearly monotonic transverse RM gradient across the core region, whose significance is  $4.6\sigma$ . We also constructed a version of this map with a circular beam, to ensure that the apparent transverse gradient was not an artefact of the low declination of the source; the RM gradient remained visible in this map, became monotonic, and had a similar significance,  $5.0\sigma$ .

**1749+096.** An RM map made from the same visibility data was published by Gabuzda et al. (2008). Our analysis shows that the previously reported monotonic, transverse RM gradient across the core has a significance is  $5.5\sigma$ . This gradient is also visible in the 8.1–15.2 GHz RM image of Zavala & Taylor (2004).

**2155–152.** An RM map made from the same visibility data was published by Mahmud & Gabuzda (2008), but without any error analysis. Mahmud & Gabuzda (2008) suggested the presence of two oppositely directed transverse RM gradients — one in the core region and one in the jet. Due to the rather different RM ranges for the core region and jet, we show separate RM maps for these two regions in Figs. 2b,c. There appears to be a transverse RM gradient across the core, but it is difficult to estimate its significance due to the elongated beam. A version of this map made with a circular beam shows a clear, monotonic RM gradient with a significance of  $5.0\sigma$ . The possible oppositely directed gradient further out in the jet reported by Mahmud et al. (2008)

is not monotonic in either the map made with the intrinsic beam or the circular beam, and we therefore do not consider it to be convincing.

## 4 DISCUSSION

### 4.1 Reliability and Significance of the Transverse RM Gradients

Table 3 gives a summary of the transverse Faraday rotation measure gradients detected in the images presented here. The statistical significances of these gradients range from  $3\sigma$  to nearly  $6\sigma$ . This indicates that these transverse RM gradients are not likely to be spurious (i.e., due to inadequacy of the  $uv$  coverage and noise): the Monte Carlo simulations of Hovatta et al. (2012) and Murphy & Gabuzda (2013) have shown that spurious gradients at the  $3\sigma$  level should arise for 4–6-frequency VLBA observations in the frequency interval considered here with a probability of no more than about 1%, with this probability being even lower for monotonic gradients encompassing differences of greater than  $3\sigma$ . Although the occurrence of spurious gradients rises substantially for VLBA observations of low-declination sources, the significances of the gradients observed across the cores/inner jets of 1334–127 and 2155–152 ( $4.5–5\sigma$ ) are high enough to make it quite improbable that these gradients are spurious.

Sign changes are observed in the transverse RM gradients detected in 0256+075, 0735+178, 0745+241 and 1652+398. This strengthens the case that these gradients are due to helical (or toroidal) magnetic fields associated with these jets, since a sign change cannot be caused by gradients in the electron density, and must be associated with a change in the direction of the line-of-sight magnetic field.

Note, however, that the absence of a sign change in the transverse RM profile does not rule out the possibility that a transverse gradient is due to a helical or toroidal field component in the region of Faraday rotation, since gradients encompassing only one sign can be observed for some combinations of helical pitch angle and viewing angle.

### 4.2 Core-Region Transverse RM Gradients

In the standard theoretical picture, the VLBI “core” represents the “photosphere” at the base of the jet, where the optical depth is roughly unity. However, in images with the resolution of those presented here, the observed core is actually a blend of this (partially) optically thick region and optically thin regions in the innermost jet. Since these optically thin regions are characterized by degrees of linear polarization that are typically a factor of 10 or more higher than at the optically thick base of the jet, they likely dominate the overall observed “core” polarization in many cases. Therefore, we have supposed that the polarization angles observed in the core are most likely orthogonal to the local magnetic field, as expected for predominantly optically thin regions. We have not observed any sudden jumps in polarization position angle by roughly  $90^\circ$  suggesting the presence of optically thick–thin transitions in the cores in our frequency ranges at the observing epochs.

Table 3: Summary of transverse RM gradients					
Source	Location	RM <sub>1</sub> rad/m <sup>2</sup>	RM <sub>2</sub> rad/m <sup>2</sup>	\Delta RM  rad/m <sup>2</sup>	Significance
0256+075 – EB	Jet	-107 ± 69	165 ± 63	272 ± 93	2.9σ
0256+075 – CB	Jet	-75 ± 46	142 ± 49	217 ± 67	3.2σ
0355+508	Core	-662 ± 109	-1283 ± 99	621 ± 147	4.2σ
0735+178	Jet	-408 ± 86	187 ± 63	595 ± 107	5.5σ
0745+241	Jet	-99 ± 15	34 ± 28	133 ± 32	4.2σ
0748+126	Core	824 ± 166	2172 ± 160	1348 ± 230	5.9σ
0820+225	Jet	26 ± 16	140 ± 30	114 ± 34	3.4σ
0823+033	Jet	-93 ± 18	-216 ± 25	123 ± 31	4.0σ
1156+295	Core	117 ± 31	345 ± 24	228 ± 39	5.8σ
1219+285	Jet	-5 ± 19	89 ± 25	94 ± 31	3.0σ
1334-127 – EB	Jet	-86 ± 48	-367 ± 37	281 ± 61	4.6σ
1334-127 – CB	Jet	-62 ± 38	-333 ± 38	271 ± 54	5.0σ
1652+398	Jet	167 ± 35	-41 ± 26	167 ± 35	4.8σ
1749+096	Core	53 ± 48	394 ± 40	341 ± 62	5.5σ
1807+698	Jet	225 ± 49	501 ± 62	276 ± 79	3.5σ
2007+777	Core	-60 ± 28	-241 ± 18	181 ± 33	5.5σ
2155-152 – CB	Core	-566 ± 13	-303 ± 50	263 ± 52	5.0σ

EB denotes elliptical beam and CB a circular beam of roughly the same area as the intrinsic elliptical beam.

This picture of the observed VLBI core at centimeter wavelengths corresponding to a mixture of optically thick and thin regions, with the observed core polarization contributed predominantly by optically thin regions, also impacts our interpretation of the core-region Faraday rotation measures. Monotonic transverse RM gradients with significances of at least  $3\sigma$  are observed across the core regions of 0355+508, 0748+126, 1156+295, 1749+096, 2007+777 and 2155-152.

The simplest approach to interpreting these gradients is to treat them in the same way as transverse gradients observed outside the core region, in the jet. While the simulations of Broderick & McKinney (2010) show that relativistic and optical depth effects can sometimes give rise to non-monotonic transverse RM gradients in core regions containing helical magnetic fields, there are also cases when these helical fields give rise to monotonic RM gradients, as they would in a fully optically thin region. In addition, most of the non-monotonic behaviour that can arise will be smoothed by convolution with a typical centimeter-wavelength VLBA beam [see, for example, the lower right panel in Fig. 8 of Broderick & McKinney (2010)]. Therefore, when a smooth, monotonic, statistically significant transverse RM gradient is observed across the core region, it is reasonable to interpret this as evidence for helical/toroidal fields in this region (i.e., in the innermost jet).

## 5 CONCLUSION

We have confirmed previous reports of transverse Faraday RM gradients across the jet structures of 7 AGNs (4.6–15.4 GHz data; Gabuzda et al. 2004, 2008), applying the error-estimation approach of Hovatta et al. (2012) and ensuring correct alignment of the polarization-angle images at the different frequencies used to construct the RM maps. Our analysis indicates all of these gradients to be monotonic and to have significances of at least  $3.4\sigma$ .

We have also investigated the reality of transverse RM

gradients visible in the previously published RM maps for 2 additional AGNs (8.1–15.2 GHz data; Zavala & Taylor 2004), which are likewise monotonic and have significances of at least  $3\sigma$ .

Finally, we have reported new monotonic transverse Faraday RM gradients with significances of  $3\sigma$  or more in another 6 AGNs for which maps were not published previously in the refereed literature (4.6–15.4 GHz data).

In all, the analysis carried out in this study has added 15 sources to the list of AGNs whose jet structures display monotonic transverse RM gradients with significances of at least  $3\sigma$ , based on the most up-to-date methods for error estimation and image analysis. One reasonable interpretation of these gradients is that they reflect the presence of helical or toroidal magnetic fields, which form due to the combination of the rotation of the central black hole and accretion disk and the jet outflow, and then travel outward with the jet material. Four of these gradients encompass RM values of both signs, strengthening the case that they are associated with a toroidal magnetic-field component, since they cannot be explained by gradients in the electron density.

It would be of interest to investigate systematic changes in the transverse RM gradients along the jet. Unfortunately, this is hindered by the superposition of a more random RM component, presumably due to turbulence in the medium surrounding the jet, through which the polarized jet radiation passes. In the few cases when a transverse RM gradient is clearly observed over a range of distances from the jet base spanning more than a beamwidth, as in 0820+225 (Gabuzda et al. 2004), 3C273 (e.g. Hovatta et al. 2012) and 3C380 (Gabuzda et al. 2014a), the gradient appears to be fairly uniform in the region where it is observed. More detailed analyses of variations in the RM gradients along the jet will be carried out in a separate study. We are also currently engaged in a project to investigate transverse RM gradients farther from the jet base than those considered here, using longer-wavelength VLBA and VLA data.

**6 ACKNOWLEDGEMENTS**

We thank Robert Zavala for providing the version of the AIPS task RM used for this work. We are also grateful to the anonymous referee for his or her quick, thorough and helpful reviews. The National Radio Astronomy Observatory is a facility of the National Science Foundation operated under cooperative agreement by Associated Universities, Inc.

**REFERENCES**

- Algaba J. C. 2013, MNRAS, 429, 3551  
 Asada K., Inoue M., Uchida Y., Kameno S., Fujisawa K., Iguchi S. & Mutoh M. 2002, PASJ, 54, L39  
 Asada K., Inoue M., Nakamura M., Kameno S. & Nagai H. 2008, ApJ, 682, 798  
 Asada K., Nakamura M., Inoue M., Kameno S. & Nagai H. 2010, ApJ, 720, 41  
 Blandford R. D. 1993, in *Astrophysical Jets* (Cambridge University Press), p. 26  
 Blandford R. D. & Königl A. 1979, ApJ, 232, 34  
 Broderick A. E. & McKinney J. C. 2010, ApJ, 725, 750  
 Burn B. J. 1966, MNRAS, 133, 67  
 Coughlan C. P. 2014, PhD Thesis, University College Cork, Ireland  
 Croke S. M. & Gabuzda D. C. 2008, MNRAS, 286, 619  
 Croke S. M., O’Sullivan S. P. & Gabuzda D. C. 2010, MNRAS, 402, 259  
 Gabuzda D. C. & Chernetskii V. A. 2003, MNRAS, 339, 669  
 Gabuzda D. C., Murray E. & Cronin P. J. 2004, MNRAS, 351, L89  
 Gabuzda D. C., Vitriřchak V. M., Mahmud M. & O’Sullivan S. P. 2008, MNRAS, 384, 1003  
 Gabuzda D. C., Cantwell T. M. & Cawthorne T. V. 2014a, MNRAS, 438, L1  
 Gabuzda D. C., Reichstein A. & O’Neill E. L. 2014b, MNRAS, 444, 172  
 Hovatta T., Lister M. L., Aller M. F., Aller H. D., Homan D. C., Kovalev Y. Y., Pushkarev A. B. & Savolainen T. 2012, AJ, 144, 105  
 Kharb P., Gabuzda D. C., O’Dea C. P., Shastri P. & Baum S. A. 2009, ApJ, 694, 1485  
 Kühn H. & Schmidt G. D. 1990, AJ, 99, 1  
 Lovelace R. V. E., Li H., Koldoba A. V., Ustyugova G. V. & Romanova M. M. 2002, ApJ, 572, 445  
 Mahmud M. & Gabuzda D. C. 2008, in *Extragalactic Jets: Theory and Observation from Radio to Gamma-ray*, ASP Conference Series 386, p. 494  
 Mahmud M., Gabuzda D. C. & Bezrukovs V. 2009, MNRAS, 400, 2  
 Mahmud M., Coughlan C. P., Murphy E., Gabuzda D. C. & Hallahan R. 2013, MNRAS, 431, 695  
 Murphy E. & Gabuzda D. C. 2013, in *The Innermost Regions of Relativistic Jets and Their Magnetic Fields*, EPJ Web of Conferences, Volume 61, id.07005 ([http://www.epj-conferences.org/articles/epjconf/abs/2013/22/epjconf\\_rj2013\\_07005/epjconf\\_rj2013\\_07005.html](http://www.epj-conferences.org/articles/epjconf/abs/2013/22/epjconf_rj2013_07005/epjconf_rj2013_07005.html))  
 Nakamura M., Uchida Y. & Hirose S. 2001, New Astronomy, 6, 2, 61  
 Pacholczyk A. G. 1970, Radio Astrophysics, W. H. Freeman, San Francisco  
 Pushkarev A. B. 2001, Astronomy Reports, 45, 667  
 Reynolds C., Cawthorne T. V. & Gabuzda D. C. 2001, MNRAS, 327, 1071  
 Rusk R. E. 1988, PhD Thesis, University of Toronto  
 Stickel M., Fried J. W. & Kühn H. 1989, A&AS, 80, 103  
 Stickel M., Fried J. W. & Kühn H. 1993, A&AS, 98, 393  
 Taylor A. R., Stil J. M. & Sunstrum C. 2009, ApJ, 702, 1230  
 Taylor G. B. & Zavala R. T. 2010, ApJ, 722, L183  
 Zavala R. T. & Taylor G. B. 2004, ApJ, 612, 749  
 Zavala R. T. & Taylor G. B. 2005, ApJ, 626, L73